Mass Transport Investigated with the Electrochemical and Electrogravimetric Impedance Techniques. 1. Water Transport in PPy/CuPTS Films

Haesik Yang and Juhyoun Kwak*

Department of Chemistry, Korea Advanced Institute of Science and Technology, Taejon 305-701, Korea

Received: September 20, 1996; In Final Form: November 18, 1996[⊗]

Water transport in poly(pyrrole/copper phthalocyaninetetrasulfonate) (PPy/CuPTS) films, where cation transport prevails, has been investigated by employing the electrochemical quartz crystal microbalance (EQCM) technique, the electrochemical impedance technique, and the electrogravimetric impedance technique. The approximate numbers of accompanying waters per cation for PPy/CuPTS films have been obtained from both cyclic EQCM experiment and impedance experiment. It is shown that the number of accompanying waters depends on the nature and concentration of an electrolyte solution as well as the redox state of the film. It increases with the hydration number of cation in an aqueous electrolyte solution and exhibits hysteresis behavior during redox cycle. It is found that ionic conductivity of cation in a film depends on the number of accompanying waters and the ion−ion interactions inside the film. It is also found that a substantial amount of water moves with the cation during the break-in process at the first cathodic scan. Moreover, the electromechanical impedance technique has been employed to verify the relation between mass and resonant frequency of an oscillating quartz crystal and to monitor morphology changes (viscoelastic change and volume change) during the redox reaction of PPy/CuPTS films. It is found that mass change can be obtained from resonant frequency without consideration of morphology changes of PPy films. It is also found that morphology changes of PPy/CuPTS films relate to the amount of water moving into or out of the film.

Introduction

Conducting polymer films such as polypyrrole (PPy), polythiophene, and polyaniline films are very attractive materials because of their unique redox, optical, and electrical properties. These characteristic properties have been applied to batteries,[1] electrochromic devices,[2] capacitors,[3] and electrochemically controlled membranes.[4] To meet the requirements of these applications, many efforts have been directed to the elucidation of charge transport mechanism. Charge transport in a film consists of electron transport and ion transport. Because ion transport in most conducting polymer films is much slower than electron transport,[5] ion transport governs their redox properties. There are two possibilities in the mode of ion transport. In the first one, reduction/oxidation of a film is accompanied by the exclusion/insertion of anion to preserve charge neutrality inside the film. In the other, cation is inserted into or excluded from the film during its redox reaction. There is also solvent transport during ion transport. It is associated with the solvation of mobile ion.

To study ion and solvent transport mechanism, the electrochemical quartz crystal microbalance (EQCM) technique[6] and the electrochemical impedance technique[7] have been widely used. In the EQCM technique, the simultaneously measured current and mass change data give important information on dominant ionic species and solvent movement. However, it is difficult to obtain quantitative and sometimes qualitative information on ion and solvent transport, because ion transport in most films is not permselective and the mode of ion transport changes as the applied potential varies. In the electrochemical impedance technique, the analysis of impedance data enables one to separate the effect of each electrochemical process from complex responses induced by various electrochemical processes and thus enables one to estimate the characteristic parameters of involved processes (i.e., diffusion coefficient). But, there is a limit to explaining impedance data in connection with the mode of ion transport because there is no information on the chemical species involved in ion transport.

The redox reaction of conducting polymer films is accompanied by mass change and optical transmittance change as well as current. Recently, the electrogravimetric impedance technique[8] and the electrooptical impedance technique[9] have been developed. The former measures small mass change for small voltage modulation, and the latter measures small transmittance change. Because mass change and transmittance change relate to only the faradaic process of a film, these techniques combined with an electrochemical impedance technique enable to separate the faradaic process of a film and other processes.[10] Moreover, the electrogravimetric impedance technique allows us to separate the contribution of anion or cation to ion transport during redox reaction and to investigate ion and solvent transport as a function of redox state.[11] Even though the technique is powerful, this has not been extensively used to study the ion and solvent transport mechanism yet. It is due to difficulty in obtaining the small sinusoidal mass change.

In the EQCM technique, mass change is obtained from the resonant frequency of an oscillating quartz crystal.[6] For the linear relation between resonant frequency and mass to be valid, the film on a quartz crystal must behave elastically. The morphology change (viscoelastic change and volume change) of a film has been observed during its redox reaction.[12] Possibly this change causes the shift of resonant frequency, leading to the erroneous determination of mass change. In order to investigate the dependence of resonant frequency on morphology change, the electromechanical impedance technique has been increasingly utilized.[13] It enables one to measure not only mass change but also morphology change.

Of conducting polymers, a PPy film is a useful system for the mechanism study of charge transport because it is easy to control the dominant ionic species of ion transport. The

* To whom correspondence should be addressed.

[⊗] Abstract published in *Advance ACS Abstracts,* January 1, 1997.

S1089-5647(96)02903-3 CCC: $14.00

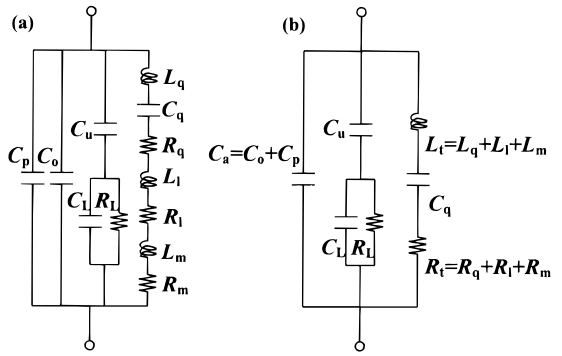

Figure 1. (a) Electrical equivalent circuit for electromechanical impedance of the quartz crystal loaded with a film and a conductive solution: C_p, parasitic capacitance; C_o, static capacitance between two electrodes; C_u, C_L, and R_L, the elements caused by electrode geometry and solution conductivity; L_q, motional inductance of quartz; C_q, motional capacitance of quartz; R_q, motional resistance of quartz; L_l, liquid-equivalent inductance; R_l, liquid-equivalent resistance; L_m, film-equivalent inductance; R_m, film-equivalent resistance. (b) Simplified electrical equivalent circuit.

dominant ionic species depend on the choice of the dopant anion incorporated during electrosynthesis and the solvent/electrolyte system employed for the redox reaction. It has been known that cation transport is dominant in the film doped with a large anion such as a poly(pyrrole/copper phthalocyaninetetrasulfonate) (PPy/CuPTS) film[14] and a polypyrrole/poly(styrenesulfonate) (PPy/PSS) film.[15] It has been also reported that the contribution of an anion to ion transport becomes small in an aqueous electrolyte solution where the anion is composed of only a divalent anion such as the sulfate ion (SO_4^{2-}).[16] It was reported that the cation is accompanied by a water during redox reaction of PPy/PSS films[15b] and PPy/CuPTS films[14] in electrolyte solutions containing a monovalent anion. But, it was difficult to measure even the approximate number of accompanying waters because the contribution of the anion is considerable in these solutions.

In this study, solvent transport for PPy/CuPTS films in aqueous electrolyte solutions has been investigated by employing the EQCM technique, the electrochemical impedance technique, and the electrogravimetric impedance technique. The electrical response (current or electrochemical capacitance) and gravimetric response (mass change rate or electrogravimetric capacitance) have been compared to clarify ion and water transport mechanism. Moreover, the relation between morphology change and resonant frequency change was checked by the electromechanical impedance analysis of the quartz crystal loaded with both a film and a liquid. First, the relation between frequency and mass in a gravimetric measurement is verified for a PPy/PSS film and a PPy/CuPTS film. Second, the number of accompanying waters per cation for PPy/CuPTS films in electrolyte solutions containing a divalent anion is investigated in terms of the nature and concentration of electrolyte solution as well as the redox state of the film. Finally, morphology change and ionic conductivity for PPy/CuPTS films are examined in connection with water transport.

Theory

Electromechanical Impedance and Resonant Frequency. The electromechanical behavior of the quartz crystal loaded with both a film and a conductive solution is represented by an electrical equivalent circuit depicted in Figure 1a, where the elements R_m and L_m are contributed by a film.[13,17] R_m is dependent upon its morphology change while L_m is dependent upon its mass. A simplified equivalent circuit in Figure 1b is used to fit electromechanical impedance data.

To characterize the electromechanical behavior of a quartz crystal, it is convenient to investigate two kinds of frequency f_r and f_s, where f_r is the maximum-conductance frequency of a quartz crystal and f_s is the zero-phase frequency of a quartz crystal.[6a,13b] f_r and f_s are approximately determined as

$$f_r = \frac{1}{2\pi}\sqrt{\frac{1}{L_t C_q}} \tag{1}$$

$$f_s = f_r\left(1 + \frac{R_t^2(C_a + C_u C_L/(C_u + C_L))}{2L_t}\right) \tag{2}$$

It shows that f_r is influenced by L_t ($=L_q + L_l + L_m$) whereas f_s is influenced by L_t and R_t ($=R_q + R_l + R_m$). Considering that L_q, L_l, R_q, and R_l are irrespective of the redox reaction of a film, L_t change and R_t change during its redox reaction correspond to L_m change and R_m change, respectively. If R_m varies during redox reaction, f_s change differs from f_r change. It has been known that resonant frequency of an oscillating quartz crystal (f_o) shows similar behavior with f_s.[13b] Thus, f_s has been used to estimate the R_m dependence of f_o. Consequently, f_r change is associated with only mass change of a film whereas f_s change and f_o change are associated with both its mass change and its morphology change.

Electrical Response vs Gravimetric Response. Assuming that mass change of a film is caused only by its redox reaction, mass change (ΔM) and mass change rate ($G = \mathrm{d}M/\mathrm{d}t$) are represented by Faraday's law as follows

$$\Delta M = -\sum \frac{W_i'}{z_i F}\Delta Q_i \tag{3}$$

$$G = -\sum \frac{W_i'}{z_i F} I_i \tag{4}$$

where

$$W_i' = W_i + Y_i W_s \tag{5}$$

In the above equations, W_i' is the molar mass of ion and accompanying solvent, z_i is the electric charge of an ion, F is Faraday constant, ΔQ_i is the charge contributed by an ion, I_i ($=\mathrm{d}Q_i/\mathrm{d}t$) is the current contributed by an ion, W_i is the molar mass of an ion, Y_i is the number of accompanying solvents per ion, and W_s is the molar mass of the solvent. The negative sign in eqs 3 and 4 is used to make mass change positive in the case that anion inserts into a film during its oxidation.

To differentiate electrochemical responses and electrogravimetric responses in impedance techniques, the terms electrochemical capacitance ($\Delta \boldsymbol{Q}/\Delta \boldsymbol{E}$), electrogravimetric capacitance ($\Delta \boldsymbol{M}/\Delta \boldsymbol{E}$), electrochemical impedance ($\Delta \boldsymbol{E}/\Delta \boldsymbol{I}$), and electrogravimetric impedance ($\Delta \boldsymbol{E}/\Delta \boldsymbol{G}$) are used. The boldface quantity is the complex representation of sinusoidal response. The relations between faradaic electrochemical responses and faradaic electrogravimetric responses are derived from eqs 3 and 4, i.e.

$$\left(\frac{\Delta \boldsymbol{M}^f}{\Delta \boldsymbol{E}^f}\right) = -\sum \frac{W_i'}{z_i F}\left(\frac{\Delta \boldsymbol{Q}^f_i}{\Delta \boldsymbol{E}^f}\right) \tag{6}$$

$$\left(\frac{\Delta \boldsymbol{E}^f}{\Delta \boldsymbol{G}^f}\right) = -\sum \frac{z_i F}{W_i'}\left(\frac{\Delta \boldsymbol{E}^f}{\Delta \boldsymbol{I}^f_i}\right) \tag{7}$$

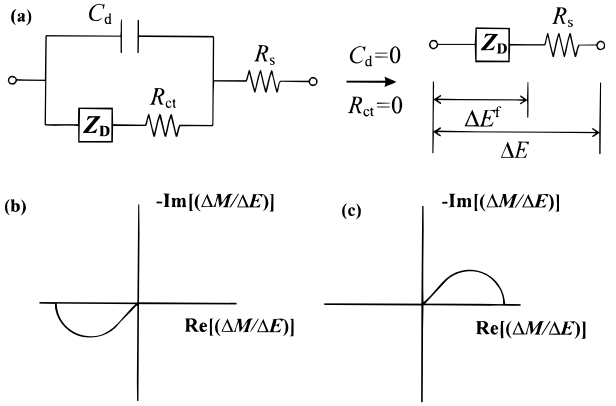

Figure 2. (a) Modified Randle's equivalent circuit: R_s, solution resistance; R_{ct}, charge transfer resistance; C_d, double-layer capacitance; $\mathbf{Z_D}$, impedance related to ion transport. Electrogravimetric capacitance plots of $\mathbf{Z_D}$ in case that ion transport is (b) cation-specific and (c) anion-specific.

Figure 2a shows the modified Randle's equivalent circuit for the electrochemical system where only one kind of ion takes part in ion transport, which is much slower than electron transport.[18] The mathematical form of the impedance $\mathbf{Z_D}$ is given by

$$\mathbf{Z}_D = R_D \frac{\coth\sqrt{j\omega R_D C_D}}{\sqrt{j\omega R_D C_D}} \tag{8}$$

where R_D is the ionic resistance in a film, C_D is the redox capacitance in a film, j is $\sqrt{-1}$, and ω is an angular frequency. Ionic conductivity in a film is calculated from $\sigma = l/R_D A$, where σ is ionic conductivity and l is film thickness.

Electrogravimetric capacitance plots for $\mathbf{Z_D}$ are shown in Figure 2b,c. The position of a electrogravimetric capacitance plot depends on ion transport mode, and its size depends on W_i'/z_i as well as C_D. When R_{ct} and C_d are very small (Figure 2a), $\Delta M = \Delta M^f$ and $\Delta Q = \Delta Q^f_i$. Without consideration of R_s, the relation between electrogravimetric capacitance and electrochemical capacitance for one ion i can be represented as follows

$$\left(\frac{\Delta \boldsymbol{M}}{\Delta \boldsymbol{E}}\right) = \left(\frac{\Delta \boldsymbol{E}^f}{\Delta \boldsymbol{E}}\right)\left(\frac{\Delta \boldsymbol{M}^f}{\Delta \boldsymbol{E}^f}\right) = -\frac{W_i'}{z_i F}\left(\frac{\Delta \boldsymbol{E}^f}{\Delta \boldsymbol{E}}\right)\left(\frac{\Delta \boldsymbol{Q}^f_i}{\Delta \boldsymbol{E}^f}\right) = -\frac{W_i'}{z_i F}\left(\frac{\Delta \boldsymbol{Q}}{\Delta \boldsymbol{E}}\right) \tag{9}$$

Experimental Section

Chemicals. Pyrrole, sodium poly(styrenesulfonate) (NaPSS), copper(II) phthalocyaninetetrasulfonic acid, tetrasodium salt (Na_4CuPTS), Li_2SO_4, Na_2SO_4, K_2SO_4, Cs_2SO_4, $MgSO_4$, D_2O, H_2PtCl_6, and KCl were purchased from Aldrich and used as received. Double-distilled water was used for the preparation of all solutions.

Electrochemistry and Film Preparation. A standard three-electrode cell was used with a Ag/AgCl reference electrode and a Pt wire counter electrode. A 6 MHz AT-cut quartz crystal (Inficon, NY) coated with Au served as the working electrode. This was clamped via an O-ring such that the area exposed to the solution is 0.32 cm^2. For ionic resistance measurement, a Au disk electrode served as the working electrode, and its electrode area is 0.02 cm^2. PPy/CuPTS films were grown potentiostatically at −0.7 V vs Ag/AgCl in an aqueous solution containing 0.02 M pyrrole and 0.01 M Na_4CuPTS. PPy/PSS films were grown at −0.6 V in a solution of 0.1 M pyrrole and 0.1 M NaPSS. The film thickness was estimated by assuming that 300 mC/cm^2 corresponds approximately to 1 μm with consideration of the reported value.[9b] Unless stated otherwise, cyclic data are those of the second cycle of two consecutive cycles after being held at the positive potential limit.

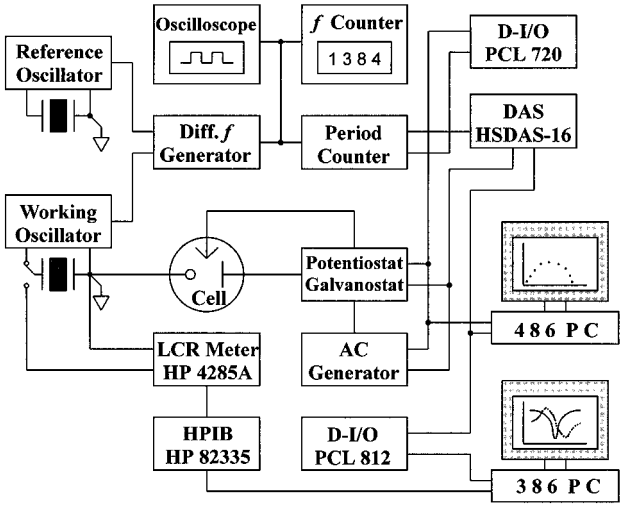

Figure 3. Schematic diagram of the experimental setup for the EQCM technique, the electrogravimetric impedance technique, the electrochemical impedance technique, and the electromechanical impedance technique.

Instrumentation and Data Treatment. The schematic diagram of the experimental setup for the EQCM technique, the electrochemical impedance technique, the electrogravimetric impedance technique, and the electromechanical impedance technique is shown in Figure 3.

The treatment of impedance data is based on fast Fourier transform (FFT) algorithm.[19] Unlike previous FFT impedance methods,[20] impedance data are obtained in not a wide frequency range but a frequency range of only 2 decades. The wide frequency range is covered by obtaining successively impedance data in several kinds of 2 decades frequency range. The perturbation signal is composed of computer-programmed sum of 12 sine signals with less than 20 mV amplitude and random phase angle. Time-domain data for electrical and gravimetric responses are simultaneously obtained by measuring current and frequency difference periodically. Electrochemical impedance data and electromechanical impedance data are fitted by using the complex nonlinear least-squares (CNLS) fitting program. The CNLS program used in this work is the LEVM program (Scribner, VA).

The EQCM calibration was carried out by coulometrically controlled platinum deposition in an aqueous solution of 10 mM H_2PtCl_6 and 0.1 M KCl. The obtained sensitivity is 4.42 ± 0.04 ng/Hz.

A more detailed description is given in the Supporting Information.

Results and Discussion

Resonant Frequency to Mass Relation. To verify the relation between f_o and mass, R_t change and three kinds of frequency change (Δf_o, Δf_r, and Δf_s) for a PPy/PSS film in an aqueous solution containing 0.5 M Cs_2SO_4 are measured during cyclic multipotential step experiment. The data for the second cycle of two consecutive cycles are shown in Figure 4b,c. The excitation signal is shown in Figure 4a. The pulse width of each step is 40 s. At each step, f_o or electromechanical impedance data (f_r, f_s, and R_t) are obtained after quiet time of 20 s. In this experiment, f_s does not exist because of large R_t.[21] However, f_s calculated by eq 2 has been used in order to

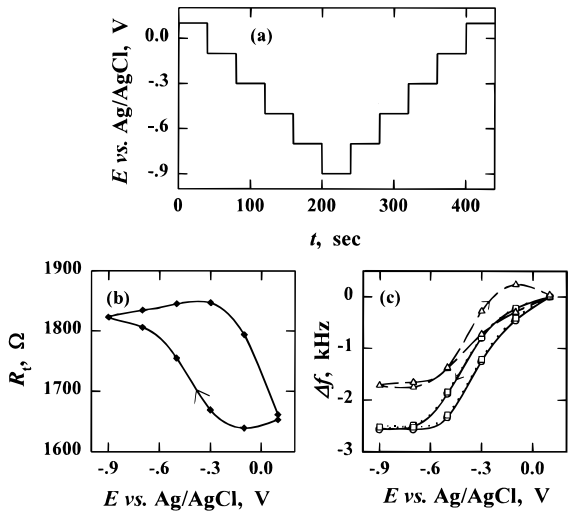

Figure 4. (a) Time to potential, (b) R_t ($=R_q + R_l + R_m$) change, and (c) f_r (○), f_o (□), and f_s (△) changes for PPy/PSS films (thickness = 1 μm) in 0.5 M Cs_2SO_4 during cyclic multipotential step.

investigate the R_m dependence of f_s and f_o.[13c,22] It is known that f_r change is associated with mass change of a film whereas f_s change and f_o change are associated with both its mass change and R_t change. In Figure 4b, R_t varies during redox cycle, leading to large difference between the f_r diagram and the f_s diagram. There are two possibilities for the dependence of f_s on R_m during f_r decrement.[13b,c] f_s decrement is smaller than f_r decrement upon R_m increasing, whereas f_s decrement is larger than f_r decrement upon R_m decreasing (eq 2). In Figure 4c, f_s decrement after cathodic scan is 850 Hz smaller than f_r decrement, because R_m increases. It has been known that f_o change is the same as f_s change.[13b,22] However, the f_o diagram is not similar to the f_s diagram, but similar to the f_r diagram.

f_o depends on the components of an oscillator circuit as well as a quartz crystal.[13b] Moreover, the large gain feedback loop in an oscillator circuit is used to obtain the stable oscillation in a system where R_t is large.[6b] Thus, the electrical equivalent circuit for a quartz crystal with an oscillator circuit is quite different from that for a quartz crystal itself. It means that the R_m dependence of f_o differs from that of f_s. From this and experimental result, it is evident that the R_m dependence of f_o cannot be estimated from the comparison between f_s change and f_r change. The comparison only between f_o change and f_r change enables one to verify the linear relation between f_o and mass. In PPy/CuPTS films, where R_m change during redox cycle is smaller than that of PPy/PSS films, there is also no significant difference between the f_r diagram and the f_o diagram. Therefore, mass change in a gravimetric experiment is obtained from f_o without consideration of morphology change of the film.

Electrical and Gravimetric Responses. In general, to investigate the correlation between electrical response and gravimetric response, mass change is compared with charge (eq 3). But, to monitor potential-dependent ion and solvent transport, it is more convenient to compare mass change rate (G) with current (I) (eq 4). Figure 5 shows cyclic voltammograms and simultaneously acquired mass change rate diagrams of PPy/CuPTS films in aqueous electrolyte solutions containing various kinds of cation and SO_4^{2-}. Assuming that ion transport is cation-specific, G is normalized by the factor $-(z_iF/W_i')$, i.e.

$$G_n = -(z_iF/W_i')G \tag{10}$$

If normalized mass change rate (G_n) is larger than I at any potential, it indicates that the actual W_i' is larger than the given W_i'. In opposite case, it indicates that the actual W_i' is smaller than the given W_i'.

In a mass change rate diagram of Figure 5a, the molar mass of Cs^+ is regarded as W_i'. In other diagrams, W_i' is fitted by adjusting the anodic peak of the mass change rate diagram to that of the cyclic voltammogram, noting that two diagrams are similar at more negative potential than −0.3 V during the anodic scan. In a Cs^+-containing solution, the difference between G_n and I is small in the overall potential range. It shows that Cs^+ transport is dominant and that the number of accompanying waters per Cs^+ (Y_{Cs^+}) is negligible. In other cation systems, the fitted W_i' is much larger than W_i, indicating that other species in addition to the cation take part in mass change. When two mass change rate diagrams in water solution and D_2O solution (Figure 5d,e) are compared, the obtained $W_i' - W_i$ at the anodic peak potential is approximately 50 and 56, respectively. The ratio of 50 to 56 corresponds roughly to that of W_{H_2O} (=18) to W_{D_2O} (=20). It confirms that the cation is accompanied by water. The Y_i values at the anodic peak potential are shown in Table 1. The sequence of Y_i is the same as that of the hydration number of alkali-metal ion in an aqueous solution.[23] In a solution containing Mg^{2+}, $Y_{Mg^{2+}}$ is 3.9, which is much larger than that for monovalent cation. In a solution containing 0.1 M Li_2SO_4, Y_{Li^+} is 4.1, which is much larger than the value 2.8 in a solution containing 0.5 M Li_2SO_4. It shows that Y_i increases as electrolyte concentration decreases. It is known that the increase in electrolyte concentration causes the decrease in dielectric constant of solution and results in the decrease in the hydration number of ion.[24] Thus, it is evident that Y_i depends on the hydration number of cation in an aqueous electrolyte solution.

In all cation systems except Cs^+, G_n and I show similar behavior at more negative potential than −0.3 V only during anodic scan. During cathodic scan, G_n is smaller than I at the first and then G_n becomes larger than I. It indicates that Y_i is uniform during exclusion of cation, whereas it gradually increases during insertion of the cation. In brief, Y_i shows "hysteresis behavior" during redox cycle. This hysteresis behavior becomes more evident as Y_i increases (Figure 5b−d). In a Mg^{2+}-containing solution (Figure 5g), hysteresis behavior is less apparent than those in Figure 5c,d while $Y_{Mg^{2+}}$ (=3.9) at anodic peak potential is larger than Y_{Na^+} (=2.4) and Y_{Li^+} (=2.8). It is due to the fact that the number of accompanying waters per unit charge of Mg^{2+} (=1.9) is smaller than 2.4 and 2.8. Thus, it can be qualitatively said that the extent of hysteresis depends on the number of accompanying waters per unit charge. In a Cs^+-containing solution (Figure 5a) of negligible water transport, G_n shows similar behavior with I during both cathodic and anodic scan. There is no apparent hysteresis behavior in this system.

In all cyclic EQCM experiments, which are those of the second cycle of two consecutive cycles, the difference between two mass values before and after redox cycle was small in comparison with mass change during anodic or cathodic scan. It indicates that the total amount of water inserted into the film during cathodic scan is similar to that excluded from the film during anodic scan. Thus, the average Y_i during cathodic scan is similar to that during anodic scan. In Figure 5h where the cathodic limit potential is −0.5 V, Y_{Li^+} at the anodic peak potential is 2.4, which is smaller than the value 2.8 in Figure 5d where the cathodic limit potential is −0.9 V. It shows that, when the cathodic limit potential is more positive, the average Y_i during anodic scan becomes smaller. It is shown that Y_i increases as cathodic scan proceeds. For this reason, the average Y_i during cathodic scan decreases as the cathodic limit potential

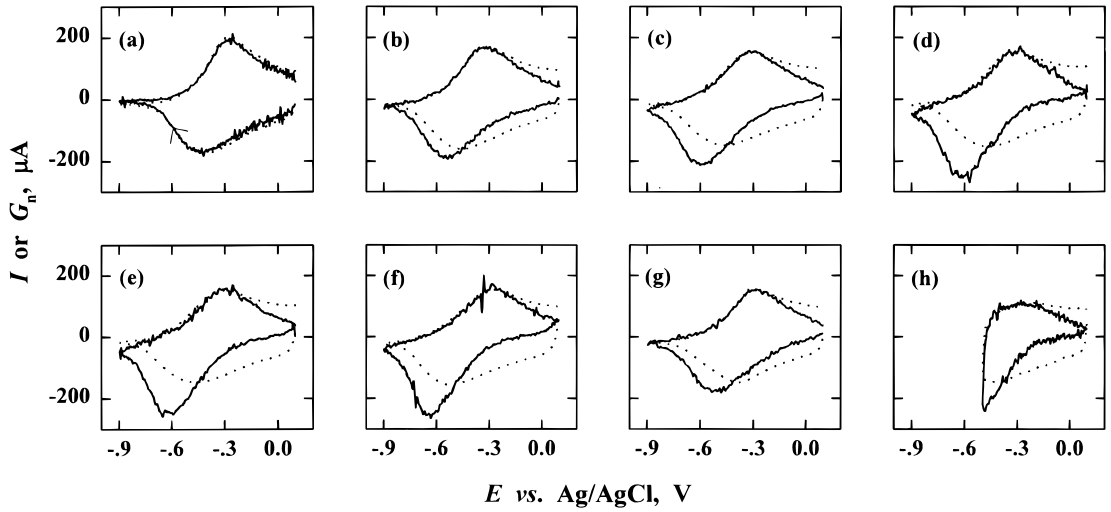

Figure 5. Cyclic voltammograms (I vs E; ···) and normalized mass change rate diagrams ($G_n = -(z_iF/W_i')G$ vs E; —) for PPy/CuPTS films (scan rate = 10 mV/s, thickness = 1 μm) in (a) 0.5 M Cs_2SO_4 ($W_i' = W_{Cs^+} = 133$), (b) 0.5 M K_2SO_4 ($W_i' = W_{K^+} + 15 = 54$), (c) 0.5 M Na_2SO_4 ($W_i' = W_{Na^+} + 44 = 67$), (d) 0.5 M Li_2SO_4 ($W_i' = W_{Li^+} + 50 = 57$), (e) 0.5 M Li_2SO_4/D_2O ($W_i' = W_{Li^+} + 56 = 63$), (f) 0.1 M Li_2SO_4 ($W_i' = W_{Li^+} + 74 = 81$), (g) 0.5 M $MgSO_4$ ($W_i' = W_{Mg^{2+}} + 70 = 94$), and (h) 0.5 M Li_2SO_4 ($W_i' = W_{Li^+} + 43 = 50$).

TABLE 1: Approximate Number of Accompanying Waters per Ion (Y_i) at Cyclic EQCM Experiment (Figure 5) and Impedance Experiment (Figure 6)

	cyclic EQCM		impedance (−0.3 V)	
solutions	$W_i' - W_i$	Y_i[a]	$W_i' - W_i$	Y_i[a]
0.5 M K_2SO_4/H_2O	15	0.8	4	0.2
0.5 M Na_2SO_4/H_2O	44	2.4	20	1.1
0.5 M Li_2SO_4/H_2O	50	2.8	22	1.2
0.5 M Li_2SO_4/D_2O	56	2.8	24	1.2
0.1 M Li_2SO_4/H_2O	74	4.1	29	1.6
0.5 M $MgSO_4/H_2O$	70	3.9	40	2.2
0.5 M Li_2SO_4/H_2O	43[b]	2.4[b]	43[c]	2.4[c]

[a] $Y_i = (W_i' - W_i)/W_s$, s = H_2O or D_2O. [b] Figure 5h. [c] Figure 6h (−0.5 V).

decreases. This results in the decrease in the average Y_i during anodic scan because the average Y_i during anodic scan is similar to that during cathodic scan. Thus, it is evident that the average Y_i during anodic scan depends on the potential range of cyclic voltammetry because of hysteresis behavior of accompanying waters.

Figure 6 shows electrochemical capacitance plots and simultaneously acquired electrogravimetric capacitance plots at the same electrolyte systems as those in Figure 5. To compare the electrochemical capacitance plot with the electrogravimetric one, the electrochemical one is normalized by the factor $-(W_i'/z_iF)$, i.e.

$$(\Delta Q/\Delta E)_n = -(W_i'/z_iF)(\Delta Q/\Delta E) \qquad (11)$$

where W_i' is fitted by adjusting a electrochemical semicircle to a electrogravimetric one except for Cs^+ case. The electrochemical capacitance plot of Figure 6a is normalized by considering only Cs^+ transport. The electrogravimetric semicircle is a little smaller than the normalized electrochemical one. It is due to the fact that there is some anion transport. In other cation systems, W_i' is larger than W_i. The difference $W_i' - W_i$ (=24) obtained in D_2O solution (Figure 6e) is larger than the difference $W_i' - W_i$ (=22) obtained in H_2O solution (Figure 6d). All shows that water transport is significant also in impedance experiments. The approximate Y_i is also shown in Table 1. In consideration of the presence of some anion movement opposite to cation movement, the actual Y_i in electrolyte solutions containing 0.5 M K_2SO_4, Na_2SO_4, and Li_2SO_4 must be larger than 0.2, 1.1, and 1.2, respectively. In a Mg^{2+}-containing solution, $Y_{Mg^{2+}}$ is larger than 2.2, which is much larger than those in solutions containing a monovalent cation. Moreover, Y_{Li^+} in a solution containing 0.1 M Li_2SO_4 is larger than 1.6, which is larger than the value 1.2 in a solution containing 0.5 M Li_2SO_4. The comparison between electrochemical capacitance and electrogravimetric capacitance also shows that Y_i increases as the hydration number of cations in an electrolyte solution increases.

In Figure 5, except part a, G_n at −0.3 V during the anodic scan is similar to I whereas G_n at −0.3 V during the cathodic scan is smaller than I, indicating that Y_i at −0.3 V during the cathodic scan is smaller than that during the anodic scan. If W_i' is adjusted to make $G_n = I$ at −0.3 V during both cathodic and anodic scans in Figure 5b,c,d,g, the fitted W_i' is shown in Table 2. The fitted W_i' in the impedance experiment (Figure 6b,c,d,g) is also shown in Table 2. For each cation system, the fitted W_i' in the impedance experiment is closer to the fitted W_i' during the cathodic scan than that during the anodic scan in the cyclic EQCM experiment. If W_i' is fitted at −0.5 V in Figure 5d, the fitted W_i' during the cathodic scan is 65 and the fitted W_i' during the anodic scan is 49, while the fitted W_i' at −0.5 V in the impedance experiment (Figure 6h) is 50. In this potential, the fitted W_i' in the impedance experiment is similar to the fitted W_i' during the anodic scan. This shows that the fitted W_i' in the impedance experiment is similar to the smaller one of two fitted W_i' in the cyclic EQCM experiment.

Break-in Process and Morphology Change. Figure 7 shows ΔR_m diagrams and mass change diagrams obtained from the electromechanical impedance analysis during the first two cycles of cyclic multipotential step for PPy/CuPTS films in solutions containing 0.5 M Cs_2SO_4, 0.5 M Li_2SO_4, and 0.1 M Li_2SO_4. During the cathodic scan, mass increases because of cation and water insertion. The increments during the first cathodic scan and the second scan are shown in Table 3. It is interesting to note that the mass increment during the first cathodic scan is much larger than that during the second scan. When more cyclic scans proceed, mass changes during subsequent cathodic scans are similar to that during the second scan.

There are two possible explanations for larger mass increment in the first cathodic scan than that in the second scan. One is that neutral salt transport takes place during the first cathodic scan, and the other is that the amount of water inserted into the

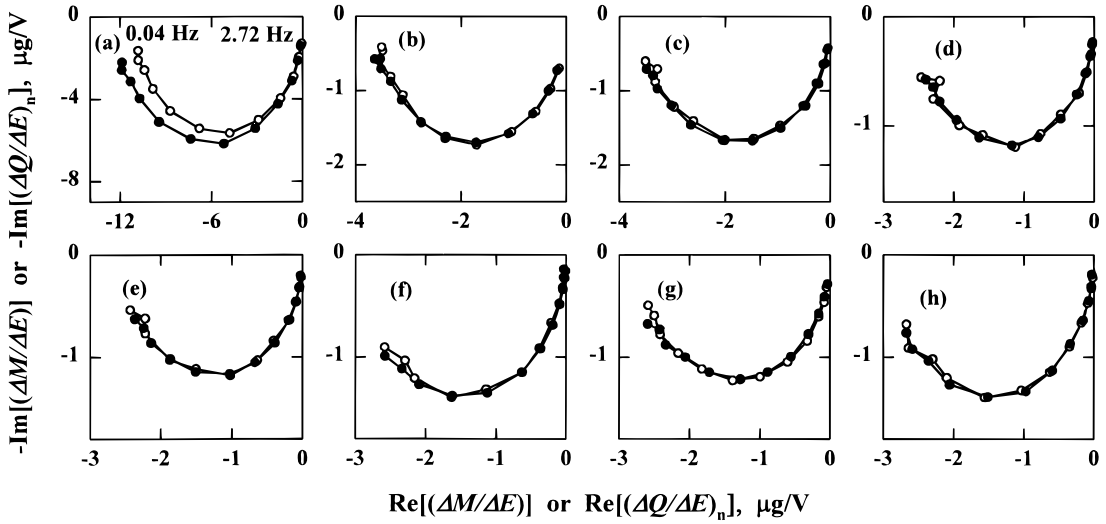

Figure 6. Electrogravimetric capacitance ($(\Delta M/\Delta E)$; ○) plots and normalized electrochemical capacitance ($(\Delta Q/\Delta E)_n = -(W_i'/z_iF)(\Delta Q/\Delta E)$; ●) plots for PPy/CuPTS films (thickness = 1 μm) at $E = -0.3$ V vs Ag/AgCl in (a) 0.5 M Cs_2SO_4 ($W_i' = W_{Cs^+} = 133$), (b) 0.5 M K_2SO_4 ($W_i' = W_{K^+} + 4 = 43$), (c) 0.5 M Na_2SO_4 ($W_i' = W_{Na^+} + 20 = 43$), (d) 0.5 M Li_2SO_4 ($W_i' = W_{Li^+} + 22 = 29$), (e) 0.5 M Li_2SO_4/D_2O ($W_i' = W_{Li^+} + 24 = 31$), (f) 0.1 M Li_2SO_4 ($W_i' = W_{Li^+} + 29 = 36$), and (g) 0.5 M $MgSO_4$ ($W_i' = W_{Mg^{2+}} + 40 = 64$), and at $E = -0.5$ V vs Ag/AgCl in (h) 0.5 M Li_2SO_4 ($W_i' = W_{Li^+} + 43 = 50$).

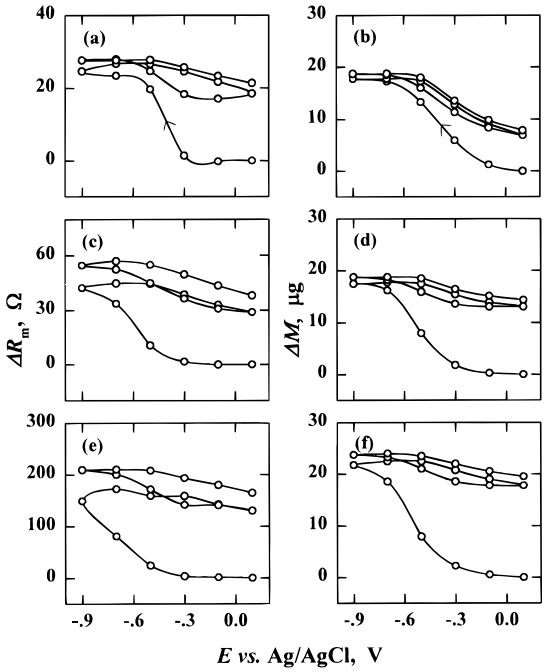

Figure 7. ΔR_m diagrams and mass change (ΔM) diagrams obtained from f_r during the first two cyclic multipotential step for PPy/CuPTS films (thickness = 1 μm) in (a, b) 0.5 M Cs_2SO_4, (c, d) 0.5 M Li_2SO_4, and (e, f) 0.1 M Li_2SO_4.

TABLE 2: Fitted Molar Mass of Ion and Accompanying Water (W_i') at Cyclic EQCM Experiment (Figure 5) and Impedance Experiment (Figure 6)

	−0.3 V				−0.5 V
	K_2SO_4	Na_2SO_4	Li_2SO_4	$MgSO_4$	Li_2SO_4
cathodic scan	36	37	28	68	65
anodic scan	54	67	57	94	49
impedance	43	43	29	64	50

film during the first cathodic scan is larger than that during the second scan. The difference between two mass increments during the first cathodic scan and the second scan is 6.0, 11.8, and 15.8 μg, respectively. The difference in a 0.1 M Li_2SO_4 solution is much larger than that in a 0.5 M Li_2SO_4 solution, while electrolyte concentration of a 0.1 M solution is higher than that of a 0.5 M solution. Moreover, the difference in a 0.5 M Cs_2SO_4 solution is smaller than those in Li^+-containing solutions, while the molar mass of Cs_2SO_4 is larger than that of Li_2SO_4. If neutral salt transport occurred, the sequence of three difference values would be reversed. On the other hand, the sequence is the same as that of the hydration number of cation in an aqueous solution. It indicates that larger mass change is due to not neutral salt transport but water transport and that the amount of water inserted into the film during the first cathodic scan is much larger than that during the second scan. It is noteworthy that the amount of water inserted into the film is considerable during the first scan even in a Cs^+-containing solution where water transport is negligible during the second cathodic scan.

TABLE 3: R_m Increment and Mass Increment during Two Cathodic Multipotential Step (Figure 7)

	0.5 M Cs_2SO_4		0.5 M Li_2SO_4		0.1 M Li_2SO_4	
ΔM and ΔR_m	1st	2nd	1st	2nd	1st	2nd
ΔM/mg	17.8	11.8	17.5	5.7	21.7	5.9
$\Delta R_m/\Omega$	25	9	42	26	149	79

It is known that a film after deposition is compact and has few free spaces.[12b,c] When a cation inserts into a film during the first cathodic scan, a very strong cathodic peak current appears at more negative potential than that during subsequent scan. This has been referred as the "break-in process".[12c,25] Thus, Figure 7 confirms that a substantial amount of water moves with a cation during the break-in process and that the amount is larger in a solution of more hydrated cation.

It is also interesting to note that R_m increases with the cathodic scan and decreases with the anodic scan. R_m increments during the first cathodic scan and the second scan are also shown in Table 3. It is known that R_m depends on volume and viscoelastic property of a film.[13c] It was also reported that volume change of polypyrrole films after redox-state switching is not large, less than 2%.[12c] Considering that R_m of a freshly deposited PPy/CuPTS film before cyclic multipotential step experiment is less than 200 Ω, ΔR_m during cathodic scan is much larger than 2%. Thus, it seems that ΔR_m is caused primarily by the viscoelastic change of a film. The R_m increment during the first cathodic scan is larger than that during the second scan. The R_m increment in a 0.1 M Li_2SO_4 solution

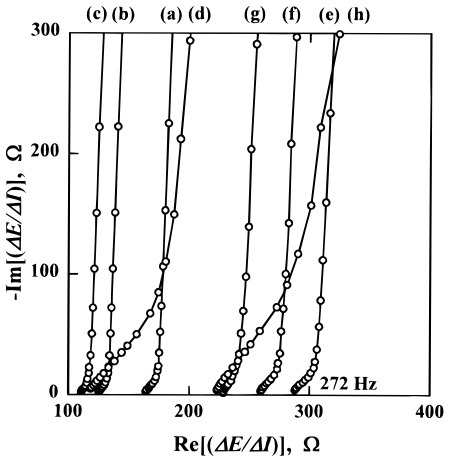

Figure 8. Electrochemical impedance ($\Delta E/\Delta I$) plots for PPy/CuPTS films (thickness = 5 μm) at $E = -0.1$ V vs Ag/AgCl in (a) 0.5 M Li_2SO_4, (b) 0.5 M Na_2SO_4, (c) 0.5 M K_2SO_4, (d) 0.5 M Cs_2SO_4, (e) 0.1 M Li_2SO_4, (f) 0.1 M Na_2SO_4, (g) 0.1 M K_2SO_4, and (h) 0.1 M Cs_2SO_4.

TABLE 4: Ionic Resistance and Ionic Conductivity Obtained from Impedance Experiment (Figure 8)

conc, M	Li_2SO_4	Na_2SO_4	K_2SO_4	Cs_2SO_4	$MgSO_4$
0.5	49[a] (5.1[b])	35 (7.1)	33 (7.6)	140 (1.8)	601 (0.42)
0.1	78 (3.2)	68 (3.7)	55 (4.5)	157 (1.6)	677 (0.37)

[a] Ionic resistance (Ω). [b] Ionic conductivity (10^{-4} S/cm).

is larger than that in a 0.5 M Li_2SO_4 solution, and the increment in a 0.5 M Cs_2SO_4 solution is smaller than those in Li^+-containing solutions.

The sequence of the R_m increment coincides with that of the amount of water inserted into the film. Moreover, in the case of Cs^+, where the amount of water moving into or out of the film during the second scan is small, the R_m increment is considerable. It shows that cation transport itself affects the morphology of the film. It is known that R_m rises upon softening or swelling of a film whereas R_m drops upon hardening or shrinking.[13b] Consequently, the insertion of cation and accompanying water makes the film soft, and the increase in the amount of water moving into or out of the film leads to the increase in its morphology change.

Ionic Conductivity. Figure 8 shows electrochemical impedance plots for PPy/CuPTS films in 0.1 and 0.5 M electrolyte solutions containing various kinds of cations. Because R_D is very small for a thin film of large surface area, it is difficult to measure R_D exactly. Thus, R_D is investigated with a thick film (5 μm) of small surface area (0.02 cm^2). Electrochemical impedance plots are composed of the 45° linear region at high frequency and the 90° linear region at low frequency.[5,18b] The value obtained by extrapolation of the linear low-frequency part of the impedance plot to the real axis corresponds approximately to $R_s + R_D/3$, and the high-frequency intercept with real axis corresponds to R_s. R_D and ionic conductivity (σ) that are obtained by fitting impedance data with the equivalent circuit of Figure 2a are shown in Table 4. The ionic conductivity obtained in a 0.1 M electrolyte solution is smaller than that in a corresponding 0.5 M electrolyte solution. It is shown in this study that Y_i increases as electrolyte concentration decreases. It is evident that the increase in Y_i causes the decrease in ionic conductivity. Moreover, ionic conductivity is cation-dependent, following the sequence $K^+ > Na^+ > Li^+ > Cs^+$. Except for Cs^+, ionic conductivity of monovalent cation is larger as Y_i is smaller. It is also interesting to note that ionic conductivity of Mg^{2+} is much smaller than that of monovalent cation, while $Y_{Mg^{2+}}$ (=2.2) is not much larger than Y_{Li^+} (=1.2) at impedance experiment (Table 1).

It is well-known that ionic conductivity in an aqueous electrolyte solution depends on the hydrodynamic radius of ion and the ion−ion interaction.[23,26] As the hydrodynamic radius of ion increases, ionic conductivity decreases because of frictional force. As electrolyte concentration increases, the ion−ion interaction increases, leading to the decrease in molar ionic conductivity. Within a conducting polymer film, electrolyte concentration is high, but the amount of existing water is small, leading to strong ion−ion interaction inside the film. Furthermore, ion pairing occurs easily because of small dielectric constant inside the film. When ion moves through the film, the movement is hindered by strong frictional force. Thus, the effect of the hydrodynamic radius and the ion−ion interaction on ionic conductivity in a film is much larger than that in an aqueous solution. It is evident that the increase in ionic conductivity with the decrease in Y_i is due to the decrease in the hydrodynamic radius. And also it seems that the low ionic conductivity of Mg^{2+} is due to not only its large hydrodynamic radius but also strong ion−ion interaction between divalent ion and charged polymer.

Conclusions

Valuable information on water transport was obtained from dynamic and steady-state behaviors of electrical and gravimetric responses for PPy/CuPTS films in aqueous electrolyte solutions. The number of accompanying waters per cation increases with the hydration number of cation in an electrolyte solution. The increase in the number of accompanying waters results in the decrease in ionic conductivity. Ionic conductivity of divalent cation is much smaller than that of monovalent cation because of strong ion−ion interaction within a film. A substantial amount of water moves with cation during the break-in process, and the amount is larger also in a solution containing more hydrated cation.

The number of accompanying waters per cation exhibits hysteresis behavior during redox cycle of PPy/CuPTS films. The number of accompanying waters is uniform during exclusion of cation, whereas it increases during insertion of cation. This hysteresis behavior is more evident as the number of accompanying waters per unit charge is larger. The number of accompanying waters at the specific potential in impedance experiment is similar to the smaller one of two numbers at that potential during cathodic and anodic scan in cyclic EQCM experiment.

Finally, morphology change of a PPy film does not affect significantly resonant frequency of an oscillating quartz crystal though it varies largely during redox cycle. The frequency to mass relation can be used in gravimetric experiments without considering morphology change of the film. The insertion of cation and accompanying water into a PPy/CuPTS film makes the film soft, and the increase in the amount of water moving into or out of the film leads to the increase in its morphology change.

Acknowledgment. This work was supported by the Korea Science and Engineering Foundation (94-0800-07-01-3).

Supporting Information Available: Details of the instrumentation, data treatment, calibration of mass sensitivity, and electromechanical admittance plot (3 pages). Ordering information is given on any current masthead page.

References and Notes

(1) Momma, T.; Nishimura, K.; Osaka, T.; Kondo, N.; Nakamura, S. *J. Electrochem. Soc.* **1994**, *141*, 2326.

(2) Hyodo, K. *Electrochim. Acta* **1994**, *39*, 265.
(3) Rudge, A.; Raistrick, I.; Gottesfeld, S.; Ferraris, J. P. *Electrochim. Acta* **1994**, *39*, 273.
(4) Ehrenbeck, C.; Jüttner, K. *Electrochim. Acta* **1996**, *41*, 511.
(5) Duffitt, G. L.; Pickup, P. G. *J. Chem. Soc., Faraday Trans.* **1992**, *88*, 1417.
(6) (a) Buttry, D. A.; Ward, M. D. *Chem. Rev.* **1992**, *92*, 1355. (b) Bard, A. J., Ed. *Electroanalytical Chemistry*; Dekker: New York, 1991; Vol. 17.
(7) (a) Southampton Electrochemistry Group. *Instrumental Methods in Electrochemistry*; Horwood: New York, 1993; Chapter 8. (b) Macdonald, J. R. *Impedance Spectroscopy*; Wiley: New York, 1987. (c) Musiani, M. M. *Electrochim. Acta* **1990**, *35*, 1665.
(8) (a) Bourkane, S.; Gabrielli, C.; Keddam, M. *J. Electroanal. Chem.* **1988**, *256*, 471. (b) Gabrielli, C.; Tribollet, B. *J. Electrochem. Soc.* **1994**, *141*, 1147.
(9) (a) Kalaji, M.; Peter, L. M. *J. Chem. Soc., Faraday Trans.* **1991**, *87*, 853. (b) Amemiya, T.; Hashimoto, K.; Fujishima, A. *J. Phys. Chem.* **1993**, *97*, 4187.
(10) Amemiya, T.; Hashimoto, K.; Fujishima, A. *J. Phys. Chem.* **1993**, *97*, 4192.
(11) (a) Cordoba-Torresi, S.; Gabrielli, C.; Keddam, M.; Takenouti, H.; Torresi, R. *J. Electroanal. Chem.* **1990**, *290*, 269. (b) Gabrielli, C.; Keddam, M.; Perrot, H.; Torresi, R. *J. Electroanal. Chem.* **1994**, *378*, 85.
(12) (a) Topart, P. A.; Noël, M. A. M. *Anal. Chem.* **1994**, *66*, 2926. (b) Pei, Q.; Inganäs, O. *J. Phys. Chem.* **1992**, *96*, 10507. (c) Pei, Q.; Inganäs, O. *J. Phys. Chem.* **1993**, *97*, 6034.
(13) (a) Martin, S. J.; Granstaff, V. E.; Frye, G. C. *Anal. Chem.* **1991**, *63*, 2272. (b) Yang, M.; Thompson, M. *Anal. Chem.* **1993**, *65*, 1158. (c) Noël, M. A. M.; Topart, P. A. *Anal. Chem.* **1994**, *66*, 484.
(14) Reynolds, J. R.; Pyo, M.; Qiu, Y.-J. *J. Electrochem. Soc.* **1994**, *141*, 35.
(15) (a) Ren, X.; Pickup, P. G. *J. Phys. Chem.* **1993**, *97*, 5356. (b) Baker, C. K.; Qiu, Y.-J.; Reynolds, J. R. *J. Phys. Chem.* **1991**, *95*, 4446.
(16) John, R.; Wallace, G. G. *J. Electroanal. Chem.* **1993**, *354*, 145.
(17) (a) Shana, Z. A.; Josse, F. *Anal. Chem.* **1994**, *66*, 1955. (b) Rodahl, M.; Höök, F.; Kasemo, B. *Anal. Chem.* **1996**, *68*, 2219.
(18) (a) Rubinstein, I.; Sabatati, E.; Rishpon, J. *J. Electrochem. Soc.* **1987**, *134*, 3078. (b) Albery, W. J.; Elliott, C. M.; Mount, A. R. *J. Electroanal. Chem.* **1990**, *288*, 15.
(19) Brigham, E. O. *The Fast Fourier Transform and its Applications*; Prentice-Hall: Englewood Cliffs, NJ, 1988.
(20) Popkirov, G. S.; Schindler, R. N. *Rev. Sci. Instrum.* **1992**, *63*, 5366.
(21) Tiean, Z.; Liehua, N.; Shouzhuo, Y. *J. Electroanal. Chem.* **1990**, *293*, 1.
(22) Topart, P. A.; Noël, M. A. M.; Liess, H.-D. *Thin Solid Films* **1994**, *239*, 196.
(23) Atkins, P. W. *Physical Chemistry*, 4th ed.; Oxford University Press: Oxford, 1990; Chapter 25.
(24) Conway, B. E.; Barradas, R. G. *Chemical Physics of Ionic Solutions*; Wiley: New York, 1966; Chapter 25.
(25) Varineau, P. T.; Buttry, D. A. *J. Phys. Chem.* **1987**, *91*,1292.
(26) Erdey-Grúz, T. *Transport Phenomena in Aqueous Solutions*; Wiley: New York, 1974; Chapter 4.